Aging in a filled polymer: Coherent small angle x-ray and light scattering

Erik Geissler,[1,*] Anne-Marie Hecht,[1] Cyrille Rochas,[1] Françoise Bley,[2] Frédéric Livet,[2] and Mark Sutton[1,3]
[1]*Laboratoire de Spectrométrie Physique, CNRS UMR No. 5588, Université Joseph Fourier de Grenoble, Boîte Postale 87, 38402 St. Martin d'Hères, France*
[2]*Laboratoire de Thermodynamique et Physico-Chimie Métallurgiques, CNRS UMR No. 5614, Institut National Polytechnique de Grenoble, Boîte Postale 75, 38402 St. Martin d'Hères, France*
[3]*Department of Physics, McGill University, 3600 University Street, Montreal, Quebec, Canada H3A 2T8*
(Received 26 June 2000)

Measurements are described using small angle coherent x-ray scattering and small angle dynamic light scattering of motion in fumed silica aggregates suspended in a poly(dimethyl siloxane) melt. At rest, this system develops weakly bound superstructures that are disrupted by mechanical stirring or thermal treatment. The observed relaxation rates correspond to a combination of liquidlike diffusion and a structural relaxation (flocculation) whereby the diffusing silica aggregates recombine into larger agglomerates at long times. Both processes are diffusion controlled. Two samples are investigated. The first, in which the silica is hydrophilic, is a highly viscous liquid for which the respective rate coefficients are about 5×10^{-14} $cm^2\,s^{-1}$ and 2×10^{-15} $cm^2\,s^{-1}$. The second sample, in which the silica surface is hydrophobic, is a thixotropic paste. The same aging mechanism in the diffusion is also observed, but with much slower rate constants, 2×10^{-15} $cm^2\,s^{-1}$ and 9×10^{-16} $cm^2\,s^{-1}$, respectively.

PACS number(s): 82.70.Gg, 82.70.Kj, 83.50.Qm, 83.70.Hq

I. INTRODUCTION

Recently there has been growing interest in x-ray correlation spectroscopy as a means of obtaining information about the dynamics of systems on a shorter length scale than is accessible with visible light [1–3]. This technique typically uses two-dimensional detectors, which have a significant additional advantage over traditional dynamic light scattering in that correlation functions of many coherence areas can be measured simultaneously. A similar multidetector approach has recently been extended to small angle light scattering [4] and can be applied to systems that either are not fully ergodic or have relaxation rates so slow that spatial averaging affords substantial time saving in improving the signal to noise ratio.

In this article we describe measurements using coherent x rays and dynamic small angle light scattering (SALS) on a slowly evolving system composed of a polymer containing finely divided silica. Such mixtures, if stored for long periods, undergo structural rearrangements (a phenomenon also known as flocculation) that, owing to a lack of suitable measurement techniques, are poorly understood on a small distance scale. Mechanical blending redisperses these superstructures.

Recently dynamic SALS measurements have been reported on colloidal gels exhibiting glassy structure, in which universal scaling behavior is observed [5]. The systems investigated here are, however, different from that in [5] in that no long range structure is present and the constituent particles can diffuse, albeit slowly, throughout the sample volume. The system we investigated is a poly(dimethyl siloxane) (PDMS) melt into which has been blended a weighed amount of fumed silica. Sample 1 contains an untreated silica (Aerosil 300, Degussa), of Brunauer-Emmett-Teller specific surface area 300 $m^2\,g^{-1}$. During the manufacturing process (i.e., prior to mixing with the PDMS) the primary silica beads, of approximate radius 5 nm, cluster irreversibly into aggregates of radius ca. 50 nm. After mixing, the hydroxylated ends of the host polymer migrate and bind to the free surfaces of the silica. This process creates starlike structures consisting of a hard core surrounded by a polymer corona. The resulting substance is a viscous liquid. A second sample contained the same quantity of fumed silica, but the surface of the latter had been previously treated with dimethyldichlorosilane to render it hydrophobic. In this second system, owing to the weakness of interaction between polymer and silica, filler aggregates attract each other and tend to form a space-filling network. In the present sample, however, since the amount of filler is below the threshold required to percolate throughout space, such a network can form only locally. The resulting solidlike paste is thixotropic, i.e., it can be deformed irreversibly by applying sufficient force, but when the force is removed the material maintains its deformed shape indefinitely.

This article describes measurements of the dynamics of these systems by means of coherent x-ray scattering spectroscopy and dynamic SALS.

II. EXPERIMENT

For the small angle x-ray scattering (SAXS) observations, the samples were placed in a cylindrical stainless steel cell with 15 μm thick mica windows, sealed with a Viton O ring. The thickness of the sample thus formed is approximately 1 mm. Measurements were conducted at the European Synchrotron Radiation Facility in Grenoble, France, on the bending magnet beamline BM2. Earlier observations are also reported of measurements made at the ID10 undulator beamline. The incident energy at both instruments was selected to be 8 keV. The incident beam from the monochromator ($\Delta\lambda/\lambda\approx1.4\times10^{-4}$) was sent first through a fast shut-

*Corresponding author.
Electronic address: erik.geissler@ujf-grenoble.fr

ter whose opening was synchronized with the data acquisition sequence of the detector, then through a 10 μm pinhole. Undesired scattering from the pinhole was removed by guard slits just before the sample. On ID10, the sample cell formed the entrance window of an evacuated flight tube, at the other end of which a lead beam stop was glued to the inside of the Kapton window immediately in front of the detector. In the arrangement on the BM2 beamline [6], the monochromatic beam was first limited by the primary slits to an aperture of 50 μm$\times$50 μm immediately after the mirror, before striking the pinhole and guard slit arrangement, the sample being located in the primary vacuum just after the guard slits. In the 10 m flight path between the primary slits and the pinhole, a differential pumping scheme eliminated the need for windows. The detector was a direct illumination charge-coupled-device (CCD) camera (Princeton Instruments), placed at 2.3 m from the sample. With this geometry, light scattered from the sample is spatially coherent over each pixel of the CCD (22×22 μm^2). To improve signal to noise ratio, the readout noise of the CCD was eliminated by means of a ''droplet'' algorithm, whereby only pixels having a content above a certain minimum threshold are counted [7].

The dynamic SALS apparatus consisted of a 2 mW HeNe laser focused on the sample and a Fresnel lens. The latter collects the light scattered by the sample and focuses it on an 8-bit CCD camera. The sample position is adjusted to maximize the size of the speckles on the detector. Images of the scattering patterns were either stored and subsequently analyzed in batch mode, or else analyzed in real time, in both cases using a multipixel multitau correlation algorithm [4]. This program, written in YORICK [8], calculates the intensity correlation function for each pixel by the multitau algorithm [9] and then sums these into subsets according the value of their transfer wave number $q=(4\pi/\lambda)\sin(\theta/2)$, where λ is the wavelength of the incident radiation and θ is the scattering angle. Having the program in the interactive language YORICK makes it highly flexible and easy to adapt.

In addition, conventional dynamic light scattering measurements were made using a standard goniometer and either a suitably attenuated 25 mW HeNe laser or a 160 mW argon ion laser (SP 1162) working at 488 nm. Light scattered into a single coherence area at different angles θ was detected by a photomultiplier, then transferred to a computer, which summed and recorded the incoming light pulses received each second over a period of many hours or even days. Intensity correlation functions were later constructed from this sequence. For the blue laser system, the scattered light was analyzed using an ALV E5000 real time correlator (ALV Langen, Germany).

The samples, kindly supplied by Rhône Poulenc Silicones, were prepared by blending 9% by weight of fumed silica with silicone oil of viscosity 20 Pa s under dry nitrogen atmosphere. The apparent viscosity of the sample containing untreated silica was approximately 500 Pa s (measured by means of a falling steel ball of diameter 1.5 mm). Within the experimental error of ca. 5%, this value was found to be independent of time and of thermal history of the sample: after heating for 24 h at 80 °C and cooling again to room temperature the measured viscosity showed no deviation from its original value.

III. THEORY

In normal binary fluid mixtures thermodynamic equilibrium is established through thermally activated concentration fluctuations that are governed by Fick's equation

$$\partial c/\partial t = D\nabla^2 c, \tag{1}$$

where D is the mutual diffusion coefficient between the two components of the binary system. Small deviations in concentration δc return to equilibrium as defined by the field correlation function

$$g(q,t)=\frac{\delta c(q,t)}{\delta c(q,0)}=\exp(-Dq^2t). \tag{2}$$

In a dynamic light scattering observation, the correlation function of the resulting intensity fluctuations is then

$$G(t)=1+\beta g(t)^2=1+\beta\exp(-2\Gamma t), \tag{3}$$

where β is the optical coherence factor of the instrument [10] and the characteristic decay rate Γ is

$$\Gamma = D\,q^2. \tag{4}$$

Equation (2) also governs the return to equilibrium from large excursions in the local concentration.

Here we consider a system in which the component particles possess an internal structure that, under a sufficiently large external force, can break down into smaller units. This situation arises in filled polymers, where filler aggregates tend to cluster into larger, weakly bound units, sometimes referred to as agglomerates. In the unperturbed state dynamic light scattering thus detects fluctuations due to the diffusion of the agglomerates. If, however, these agglomerates have been disrupted or dispersed by an external perturbation such as stirring, the individual aggregates become temporarily more mobile owing to their smaller hydrodynamic radius. After removal of the perturbation, the system returns to its equilibrium state with some time constant for structural reorganization τ_{SR}. Thus, after a mechanical perturbation, we expect to observe a temporary increase in the diffusion rate. In such an idealized situation therefore,

$$\Gamma = Dq^2[1+a\exp(-t_0/\tau_{SR})], \tag{5}$$

where the factor $(1+a)$ describes the enhancement in diffusion rate due to fragmentation, and t_0 is the time elapsed since the mechanical perturbation ceased. We make the additional, but important, assumption that the structural recovery of the agglomerates also obeys a diffusion equation, with a proportionality coefficient D_{SR}. The latter need not necessarily be the same as that describing the translational motion either of the aggregates or of the agglomerates. Thus

$$1/\tau_{SR}=D_{SR}q^2 \tag{6}$$

and hence

$$\Gamma = Dq^2[1+a\exp(-D_{SR}q^2t_0)]. \tag{7}$$

Insofar as D_{SR} may be different from D, the former describes the rate of accretion of the internal structure.

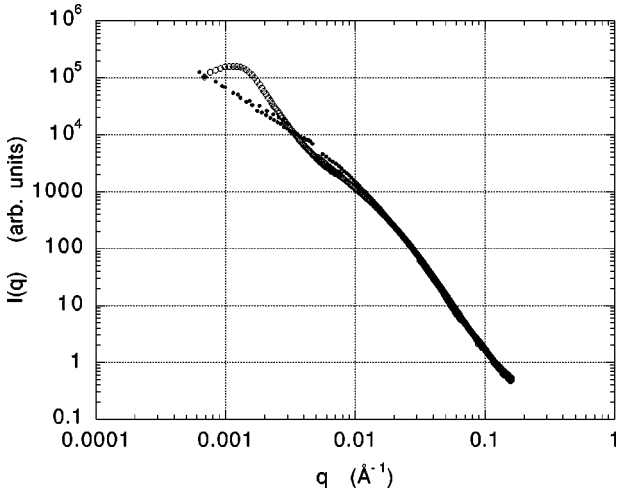

FIG. 1. SAXS spectrum for samples 1 (open circles) and 2 (filled circles). Sample 1 is composed of a 9% w/w suspension of untreated fumed silica (Aerosil 300) in polydimethyl siloxane, while sample 2 contains the same weight fraction of hydrophobized silica. These data, obtained at ESRF beamline BM2, are regrouped from the two-dimensional image of the CCD detector.

IV. RESULTS AND DISCUSSION

The static SAXS spectra $I(q)$ of samples 1 and 2 are displayed in Fig. 1. The former exhibits an intensity maximum, characteristic of interparticle interference in a system with liquidlike order. The position of this maximum, determined in a Kratky plot $q^2I(q)$ vs q, is $q_m \approx 1.6 \times 10^{-3}$ Å^{-1}, corresponding to an interparticle distance of $2\pi/q_m \approx 400$ nm. No analogous order peak is visible in sample 2. It is noteworthy that the signal from a sample consisting of pure dry filler (i.e., in the absence of a PDMS matrix) displays no such peak. Owing to its greater electron density contrast, the last system scatters many times more strongly and is therefore more liable to multiple scattering than either sample 1 or 2. The possibility that the order peak observed in sample 1 is an experimental artifact related either to multiple scattering or to detector saturation must therefore be discounted.

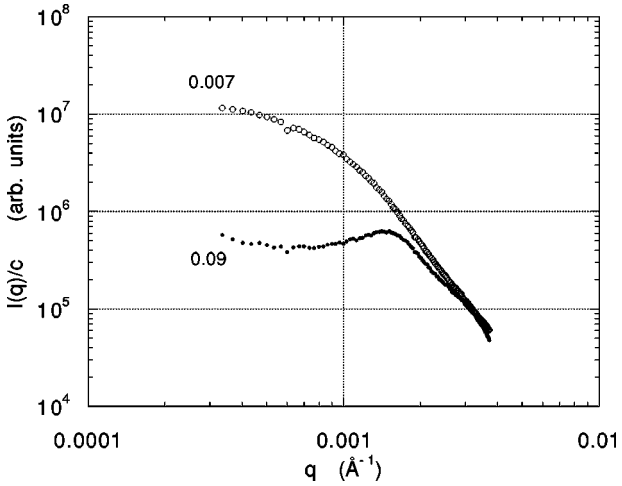

FIG. 2. Normalized intensity $I(q)/c$ of visible light ($\lambda = 488$ nm) scattered from sample 1 (lower curve). The upper curve is obtained from a specimen of sample 1 diluted in PDMS oil to a silica weight fraction 0.007. The radius of gyration calculated from the latter curve is $R_G = 185$ nm.

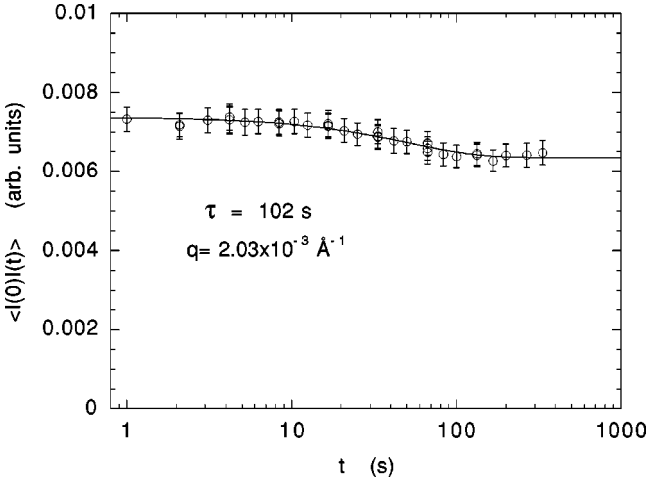

FIG. 3. Unnormalized SAXS intensity correlation function of signal scattered from the same sample as in Fig. 1 for $q = 2.03 \times 10^{-3}$ Å^{-1}. The continuous curve through the data points is the least squares fit to Eq. (9). Data collected on ID10.

Figure 1 contains structural information that has a bearing on the dynamics of this system. At high q both curves tend to an asymptotic straight line behavior with slope -4, characteristic of surface scattering from the primary particles in the aggregates [11]. In the low q range, however, the data from sample 2 appear to be linear with a slope close to -1.6. Such fractal-like behavior is consistent with the phenomenon of cluster-cluster aggregation; a fractal dimension less than 1.8 indicates a more open structure with weak bonding [12]. To understand sample 1, on the other hand, measurements must be extended to even smaller values of q. Figure 2 shows static light scattering observations of this system, in which the same intensity maximum is observed as in Fig. 1. When this sample is diluted in excess PDMS oil, however, the modulation of the signal due to the interaggregate structure factor disappears and the intensity, instead of exhibiting a maximum, rises to a plateau at small q. The signal from the dilute sample is simply proportional to the scattering form factor of the component aggregates. The radius of gyration found from the plateau region, $R_G = 185$ nm, is consistent with the interparticle distance noted above.

Figure 3 shows the unnormalized SAXS intensity correlation function

$$\langle I(0)I(t)\rangle = \langle I\rangle^2 G(t), \tag{8}$$

obtained on ID10 for $q = 0.002$ Å^{-1} in sample 1. The continuous curve through the points is

$$\langle I(q,0)I(q,t)\rangle = c_0 + c_1 \exp(-2t/\tau) = c_0 G(t), \tag{9}$$

in which $I(q,t)$ is the scattered intensity at time t, and the angular brackets indicate an average over the experimental accumulation time as well as over all pixels with the same value of q. The amplitudes c_0 and c_1 and the relaxation time τ in Eq. (9) are found by nonlinear least squares fitting. As these measurements are made under homodyne conditions [10], the ratio c_1/c_0 corresponds to the optical coherence factor of the detection system, i.e., $\beta \approx 0.16$. (Higher values

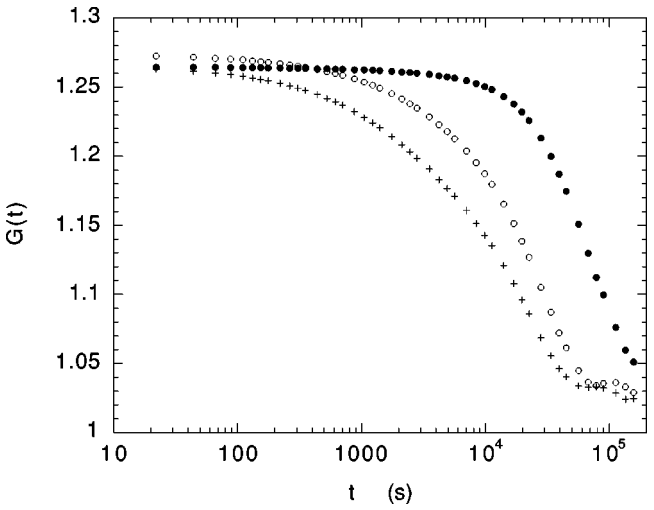

FIG. 4. Unnormalized dynamic SALS intensity correlation functions from sample 1. The values of q are ●, 7.6×10^{-5} Å^{-1}; ○, 1.8×10^{-4} Å^{-1}; +, 2.4×10^{-4} Å^{-1}.

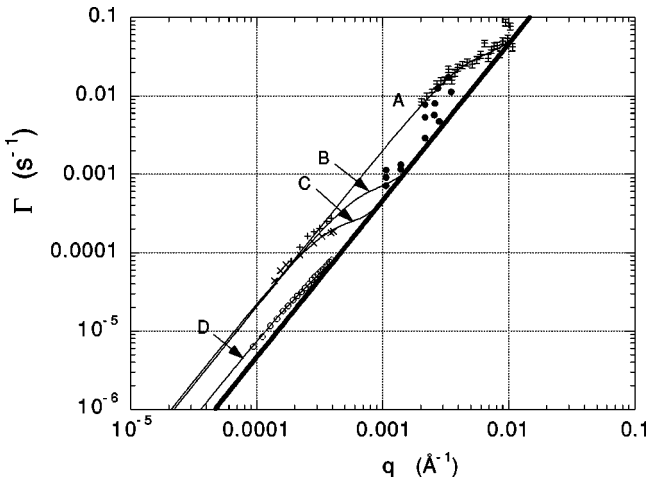

FIG. 5. Decay rate $\Gamma(q)$ measured by coherent x-ray scattering (+ with error bars), wide angle dynamic light scattering (●), and SALS (+, 24 h after heating; ×, 72 h after heating; ○, 6 days after mechanical mixing). The thick line with slope 2 defines the diffusion rate in the unperturbed system [Eq. (10)]. Continuous lines A–D are the fits to Eq. (7).

of β are now routinely obtained on the ID10 beamline since these measurements were performed. The value of β, however, in no way affects the results.)

Figure 4 shows results of equivalent measurements made on the same sample by dynamic SALS. In this figure the correlation functions for several angles are shown. The mean relaxation rates $\Gamma(q)=1/\tau$ from SAXS and SALS are displayed in Fig. 5. This figure also includes observations made at larger angles θ with a standard dynamic light scattering apparatus (filled circles) using a goniometer equipped with a photomultiplier. The latter data, obtained sequentially from a single coherence area, display considerable scatter; these results depend on the time at which the measurements were made. It can be seen, however, that the data points from all three techniques lie either on or above a limiting line (heavy line in the figure), characteristic of a diffusive motion, i.e., having a slope 2 in the double logarithmic plot. This boundary is defined by Eq. (2) where

$$D=4.6\times10^{-14}\ \text{cm}^2\,\text{s}^{-1}\quad(\text{sample 1}).\tag{10}$$

The striking feature of Fig. 5 is that the relaxation rates measured by coherent SAXS and SALS are not proportional to q^2, but tend asymptotically at large q toward the relaxation rate defined by Eq. (10). In both these techniques, unlike conventional photon correlation spectroscopy using a single photomultiplier, data from the area detector are collected for all angles simultaneously. Each data set therefore corresponds to the same delay time t_0 after the mechanical perturbation is introduced during sample preparation.

The present measurements thus provide a test of the model defined by Eq. (7) and hence can be used to determine D_{SR}. The fits of Eq. (7) through four different data sets are displayed as thin lines in Fig. 5. Good general agreement with the measurements is found. Furthermore, substitution of Eq. (6) by a q dependence weaker than $\tau_{SR}\propto q^{-2}$ fails to reproduce the shape of the curves in Fig. 4. For the dynamic SALS measurements, performed after delays of 1 day and 3 days (curves B and C), the values found for $D_{SR}t_0$ are equal to 1.8×10^{-10} cm^2 and 5.5×10^{-10} cm^2, respectively. Division by the corresponding delay time yields for these two results

$$D_{SR}\approx2.1\times10^{-15}\ \text{cm}^2\,\text{s}^{-1}\quad(\text{sample 1 SALS}).\tag{11}$$

For the SAXS measurements, the curve denoted by A in Fig. 5 corresponds to Eq. (7) with $D_{SR}t_0=3.7\times10^{-12}$ cm^2. Although this sample comes from the same batch, its history is different from the light scattering situation where the specimen is inserted into a rigid quartz cell and thereafter left undisturbed. For the present SAXS observations the sample is inserted into a cell with thin mica windows, which deform as soon as the sample chamber is evacuated at the start of the experiment. The time at which the specimen is prepared thus overestimates the effective recovery time t_0. The uncertainty is further compounded by possible ionizing effects of the x-ray beam, which may introduce additional perturbation. The estimated value $t_0\approx3600$ s in this case should therefore be viewed with caution. With this rider, the resulting value

$$D_{SR}\approx1.0\times10^{-15}\ \text{cm}^2\,\text{s}^{-1}\quad(\text{sample 1 SAXS})\tag{12}$$

is roughly half that found from dynamic SALS. This result suggests that the x-ray beam at ID10 probably did perturb the system, thus making the effective delay time shorter than the estimated value 3600 s. (Direct evidence for this perturbation is provided by the fact that exposure of the sample to the x-ray beam for more than a few thousand seconds caused significant radiation damage, revealed by a large increase in the measured relaxation rates Γ.) It is also noteworthy that the empirical parameter a introduced in Eq. (6) to model the amplitude of the perturbation is approximately equal to 4 both for the SAXS data and in the SALS curves B and C, where the specimen was heated to 80 °C in order to remove bubbles. For curve D, where no heating was employed, the value of a is approximately 0.7. These results suggest that

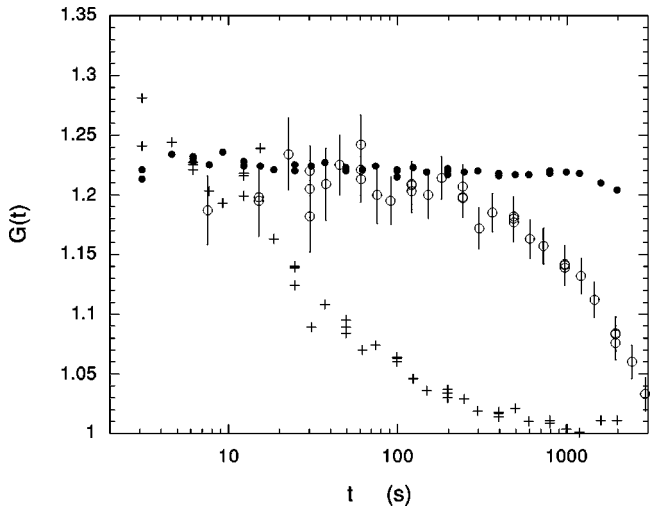

FIG. 6. SAXS intensity correlation functions at $q=1.71\times10^{-3}$ Å^{-1} for dry aerosol (●), sample 1 (+), and thixotropic sample 2 (○). The value of the optical coherence factor β is approximately 0.23. (Data obtained on BM2.)

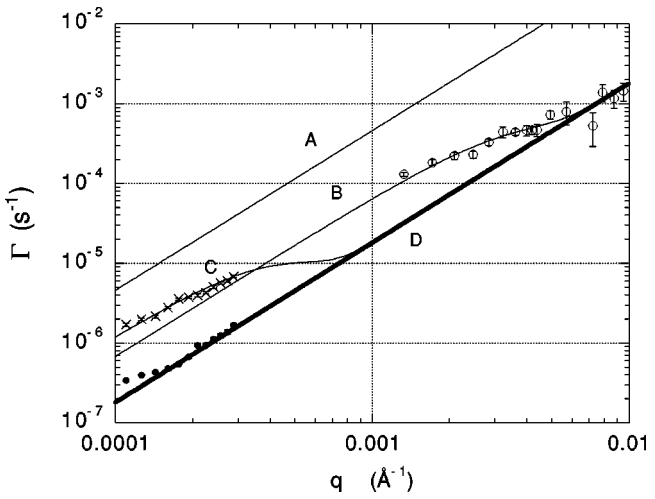

FIG. 7. Decay rate $\Gamma(q)$ from sample 2 measured by coherent SAXS (○, $t_0=10^4$ s) and SAL scattering (×, $t_0=7\times10^5$ s; ●, $t_0=10^6$ s). Curves *B* and *C* are the fits of Eq. (7) through the data points; *D* is the equilibrium relaxation curve for this system, $\Gamma=1.8\times10^{-15}$ cm^2 s^{-1}. For comparison, the unperturbed diffusion curve of sample 1 is shown (curve *A*).

heating or exposure to x rays may produce more disruption than the simple mechanical disturbance incurred by transferring the sample into its cell.

Sample 2 exhibits analogous behavior to sample 1, but the observed relaxations are considerably slower. As an illustration, Fig. 6 shows a comparison of coherent SAXS measurements performed at BM2 on three different samples. Correlation functions at $q=1.6\times10^{-3}$ Å^{-1} are displayed for (i) the dry aerosol powder, (ii) sample 1, and (iii) sample 2. These measurements show that sample 2, in spite of its thixotropic behavior and apparent immobility on a macroscopic scale, exhibits diffusional motion with a time constant that is more than an order of magnitude longer than that of sample 1. These SAXS results, together with dynamic SALS measurements performed on the same thixotropic sample, are shown in Fig. 7. The asymptotic diffusion coefficient, indicated by the heavy line in Fig. 7, is in this case

$$D\approx1.8\times10^{-15}\ \text{cm}^2\,\text{s}^{-1}\quad(\text{sample 2}),\tag{13}$$

i.e., some 25 times slower than for sample 1. Owing to the lower emitted intensity at the bending magnet source BM2 (ca. 2×10^6 photons/s transmitted through the 10 μm diaphragm), the disruptive effect of the x-ray beam on the structure of the sample is expected to be less pronounced than with the undulator source ID10. The fits drawn through the data points in Fig. 7 correspond to values of $D_{SR}t_0=9\times10^{-12}$ cm s^{-1} and 6.3×10^{-10} cm s^{-1} for SAXS and SALS, respectively, while the estimated recovery times in these two cases were 10^4 s and 7×10^5 s, respectively. Both of these measurements thus yield the same estimate for the diffusion coefficient of the structural repair mechanism, namely,

$$D_{SR}\approx9\times10^{-16}\ \text{cm}^2\,\text{s}^{-1}\quad(\text{sample 2}).\tag{14}$$

V. CONCLUSIONS

Coherent x-ray and small angle light scattering observations demonstrate that aging by structural relaxation, in addition to mutual diffusion, is an important factor in polymer melts containing fumed silica. Two samples were investigated here. One, containing hydrophilic silica, is a viscous liquid whose viscosity $\eta\approx500$ Pa s is independent of time and of its thermal history. By virtue of the Stokes-Einstein relationship, the observed time- and *q*-dependent effects in the diffusion properties are thus attributed to changes in the superstructure: after disruption by mechanical and/or thermal treatment the silica agglomerates slowly reassemble. A second sample, containing hydrophobic silica, is thixotropic, i.e., the viscosity measured by the falling bead technique is immeasurably large. In this sample both self-diffusion and structural reorganization occur nevertheless, in a manner analogous to that in the liquid system. In both these samples, the small angle x-ray and light scattering responses indicate that in the equilibrium state the aggregates are only weakly bound to each other.

In the *q* range investigated, the structural relaxation obeys Fick's equation, i.e., it is diffusion controlled. The corresponding diffusion coefficient D_{SR}, for the system containing untreated silica, is more than an order of magnitude smaller than *D*, the diffusion rate of the particles in the suspension. For the thixotropic sample, both *D* and D_{SR} are of the same order of magnitude as observed for D_{SR} in the liquidlike system.

Finally, the results show that scattering techniques based on multidetectors, particularly coherent x-ray scattering, allow these extremely slow motions to be measured in a relatively short time span.

ACKNOWLEDGMENTS

We are grateful to the ESRF for access to beamlines BM2 and ID10. We also express our gratitude to Jean-François Bérar, Gerhard Grübel, and Françoise Ehrburger-Dolle for helpful advice and fruitful discussions.

[1] M. Sutton, S.E. Nagler, S.G.J. Mochrie, T. Greytak, L.E. Bermann, G. Held, and G.B. Stephenson, Nature (London) **352**, 608 (1991).
[2] S.G.J. Mochrie, A.M. Mayes, A.R. Sandy, M. Sutton, S. Brauer, G.B. Stephenson, D.L. Abernathy, and G. Grübel, Phys. Rev. Lett. **78**, 1275 (1997).
[3] F. Livet, F. Bley, R. Caudron, E. Geissler, D. Abernathy, C. Detlefs, G. Grübel, and M. Sutton (unpublished).
[4] L. Cipelletti and D.A. Weitz, Rev. Sci. Instrum. **70**, 3214 (1999).
[5] L. Cipelletti, S. Manley, R.C. Ball, and D.A. Weitz, Phys. Rev. Lett. **84**, 2275 (2000).
[6] J.P. Simon, A. Arnaud, F. Bley, J.F. Bérar, B. Caillot, V. Comparat, E. Geissler, A. de Geyer, P. Jeantey, F. Livet, and H. Okuda, J. Appl. Crystallogr. **30**, 900 (1997).
[7] F. Livet, F. Bley, A. Létoublon, J.P. Simon, and J.F. Bérar, J. Synchrotron Radiat. **5**, 1337 (1998).
[8] D.H. Munro, Comput. Phys. **9**, 609 (1995).
[9] K. Schätzel, in *Dynamic Light Scattering*, edited by W. Brown (Clarendon Press, Oxford, 1993), Chap. 2.
[10] B.J. Berne and R. Pecora, *Dynamic Light Scattering* (Wiley, New York, 1976).
[11] O. Glatter and O. Kratky, *Small Angle X-ray Scattering* (Academic, London, 1982).
[12] R. Jullien, Comments Condens. Matter Phys. **13**, 177 (1987).